AAS 16-499

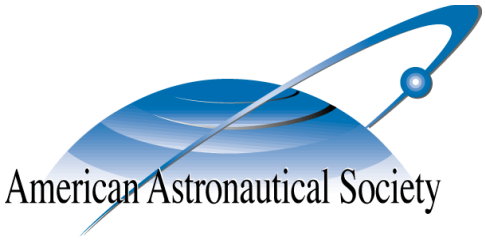

American Institute of
Aeronautics and Astronautics

DYNAMICS AND CONTROL OF THE FLEXIBLE ELECTROSTATIC SAIL DEPLOYMENT

JoAnna Fulton and Hanspeter Schaub

AAS/AIAA 26th Spaceflight Mechanics Meeting

Napa, California **February 14-18, 2016**

AAS Publications Office, P.O. Box 28130, San Diego, CA 92198

AAS 16-499

DYNAMICS AND CONTROL OF THE FLEXIBLE ELECTROSTATIC SAIL DEPLOYMENT

JoAnna Fulton* and Hanspeter Schaub†

The deployment dynamics of a radially configured, spin stabilized, electrostatic sail (E-sail) are modeled for a hub-mounted control actuator. Spacecraft hub control torque requirements for obtaining desired system spin rate trajectories are investigated. The dynamics are treated as a planar deployment and feedback control is applied with a PID controller. The sail is modeled for two different deployment strategies and tether stowage configurations, a tether spool wound up on a cylindrical hub which deploys the tether end masses tangentially, and a radially deployed configuration where each tether is stowed on an individual hub and actuated by a spool motor. The advantages and challenges of each deployment strategy are discussed. Additionally, deployment durations and torque capability requirements are determined for several tangentially deployed E-sails with varying characteristics.

INTRODUCTION

This paper aims to develop a characterization of the controlled deployment for the electrostatic sail, or electric sail (E-sail). The E-sail is a novel propellantless in-space propulsion concept with great potential for fast interplanetary and near interstellar missions, invented and proposed by Pekka Janhunen[1] at the Finnish Meteorological Institute. In this concept, a system of radially configured, thin, charged tethers generate an electric field that interacts with solar wind protons to harvest acceleration for spacecraft propulsion, demonstrated in Figure 1. This provides infinite specific impulse and eliminates the need for traditional chemical propellants,[2] where only an electron gun is required to maintain the electrostatic charge on the tethers. This solar wind propulsion concept is advantageous in comparison to the solar radiation pressure (SRP) based solar sail due to the effective area of the electrostatic forces and improved solar radius dependence.[3] A single charged wire, microns thick, will create a meters-wide effective area, expanding the area of influence of a minimal structure. In comparison, SRP is directly dependent on the physical area of the solar sail, providing many challenges in manufacturing, packaging, and deploying large membranes.[4] The solar radius dependence of the E-sail has been shown to decay the acceleration at $1/r^{7/6}$, slower than that of the solar sail at $1/r^2$. This is encouraging for long distance missions to the outer planets and beyond. However, the E-sail is not operable within a planet's magnetosphere, where the solar wind protons are deflected, whereas a solar sail still accelerates on the photons in this region.

Multiple missions have been designed using the E-sail as the primary propulsion system with encouraging results. A fast entry probe mission to Uranus could be achieved in less than 6 years,[6]

*Graduate Research Assistant, Aerospace Engineering Sciences, University of Colorado at Boulder, 431 UCB, Colorado Center for Astrodynamics Research, Boulder, CO 80309-0431

†Alfred T. and Betty E. Look Professor of Engineering, Aerospace Engineering Sciences, University of Colorado at Boulder, 431 UCB, Colorado Center for Astrodynamics Research, Boulder, CO 80309-0431

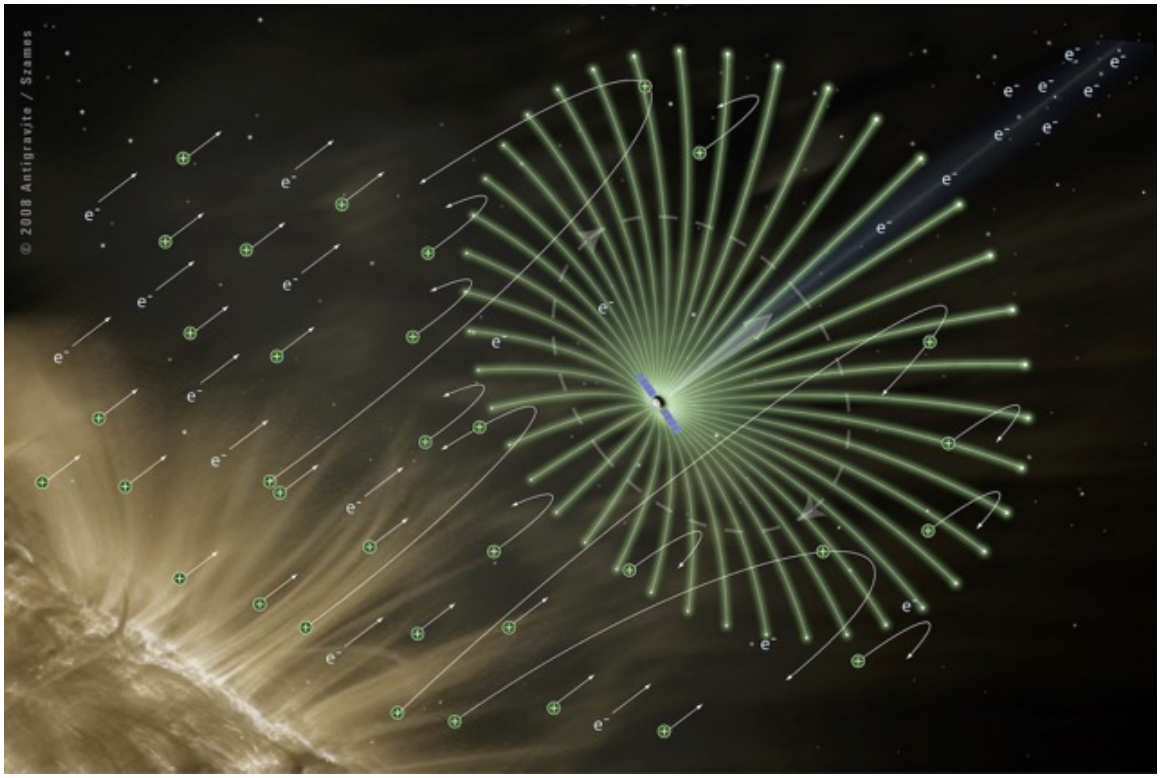

Figure 1. The electrostatic sail is charged by a spin axis-pointed electron beam and deflects solar wind protons to generate thrust. Artist concept image by A. Szames.[5]

the interstellar medium reached in as little as 10 years,[7] and a near Earth asteroid rendezvous could be completed within a year.[8] Additionally, missions to the inner planets, such as Venus and Mars, could also be achieved in less than 1 and 2 years, respectively.[9] This provides adequate motivation to pursue further development of the E-sail system. The electrostatic propulsion theory enabling these missions has been thoroughly studied. However, the coupled dynamics of the spacecraft and charged tether system is not well understood. Typically, the E-sail systems considered are composed of 50-100 tethers, 10-30 km in length, with payload masses of 100-1000 kg. These tethers are constructed using multiple micron-thick conductive tethers with auxiliary loops, known as a Hoytether,[10] to provide redundancy and protect against micrometeors. Construction of such tethers at the desired length has been investigated with encouraging results.[11] One such tether, 10 meters in length, was flown on the EstCube-1[12] but was not deployed.[13] Despite this, evidence supporting the feasibility of the E-sail is continuing to develop, and steps will now be taken towards understanding the deployment requirements for such a structure.

During flight, the tethers are spin-stabilized to maintain tensioned, radial, straight line configurations. Therefore, the deployment scheme must settle with the spacecraft and each tether component rotating at equal rates. However, a mass spinning out from a central body will dramatically change the body rates as momentum is exchanged from the body to the deploying mass. For example, a spacecraft-tether system modeled with a spherical pendulum (such as a yo-yo despinner) will asymptotically approach the negative initial rate if left in free spin. Therefore, energy and momentum must be continually input to the system as the tethers are deploying to prevent large deviations

in spin rates. A primary challenge for the E-sail deployment is determining a low-risk scheme to accomplish this, presenting a non-trivial task.

A proposed scheme for the E-sail mounts the tethers at a radial orientation, where each tether is housed with an individual hub and motor subsystem to conduct the tether unspooling. An auxiliary tether would line the periphery of the sail, and thruster units would interface between the tether end points and auxiliary tether to control position and momentum. These components significantly increase the mass budget of the E-sail and introduce a highly complex dynamics problem. In this paper, an alternative E-sail configuration is investigated, where no auxiliary tether is used and only small end masses are mounted at the tips. This would greatly reduce the mass budget of the E-sail system. Additionally, novel deployment schemes are proposed, where the control will be actuated using hub-mounted devices such as electric thrusters. Doing so will eliminate the difficulty of coordinating and commanding multiple systems. Furthermore, applying torque through the hub can be done using commercially available products, whereas tether end point thruster units are currently under development.

Two deployment schemes of this type are considered. The first is a tangentially aligned deployment, where all tethers are mounted on a central hub oriented with the spacecraft hub spin axis, taking advantage of the rotational dynamics to deploy the tethers simultaneously. This method requires further engineering development with regard to how such a system would be designed, where methods such as stacking each tether in parallel may be feasible but have not be tested. The second deployment scheme uses a radially oriented deployment configuration. The dynamic behavior, energy requirements, and control stability of these two methods are compared. The coupled rotational dynamics of the spacecraft hub and E-sail system is modeled during the deployment phase and the control of these dynamics is investigated. The deployment is assumed to occur in a single plane, reducing the problem to rotational degrees of freedoms about the out of plane axis and ignoring out of plane dynamics. It is also assumed that the spacecraft has reached deep space conditions before initiating deployment, the sail is not charged during deployment, and the tethers do not stick or adhere as they deploy.

TANGENTIAL AND RADIAL DYNAMICS MODELING

Spacecraft and E-Sail Mass Model

The mass budget of the E-sail and spacecraft system is selected such that the characteristic acceleration of the E-sail at 1 Au from the Sun is between $a_\oplus = 0.1 - 1$ mm s^{-2}. At $a_\oplus = 1$ mm s^{-2}, significantly faster missions to the outer planets and beyond are feasible.[6] The characteristic acceleration is given by:[14]

$$a_\oplus = \frac{fNL}{m} \tag{1}$$

where N is the number of tethers, L is the length of the tethers, m is the total mass of the spacecraft, and f is the thrust per unit tether length at 1 AU from the Sun. Using the physical reference data given for the E-sail,[14] this is known to be $f = 579.84$ nN m^{-1} for an E-sail operating at 25 kV nominal tether voltage. The total system mass is set to $m = 500$ kg, a smaller but feasible mass for an interplanetary science mission, to facilitate greater focus on the other free parameters of the system. It is assumed that the maximum number of tethers is 100 and the maximum length of a tether is restricted to 20 km.[14] However, this only slightly restricts the range of E-sail sizes that will yield the desired characteristic acceleration in (1). The significance of these parameters is explored in considering the system inertia and momentum in later sections of the paper.

Accurate modeling of the E-sail deployment requires that the tethers are not treated as massless sub-structures. For a scenario where there is minimal end mass, no remote devices, and minimal number of tethers with maximum length, the tethers themselves are the largest contribution to the spacecraft system momentum. Therefore, tether inertia is no longer negligible and is modeled as a slender rod with total mass equal to the system mass. This model assumes the tether remains straight, but future models will include discrete points of freedom to increase the fidelity of the flexible body dynamics model. The tether mass is described as a function of the deployment length, where the mass per unit length per tether is assumed to be $\lambda = 1.155 \times 10^{-5}$ kg/m.[14] Where ρ is the mass per unit length for N number of tethers, $\rho = N\lambda$ for a given sail size. The mass of all deploying tethers is then described as:

$$m_T = \rho l = \rho R \phi \tag{2}$$

where l is the deployed length, which can be described in terms of the unwrap angle ϕ and the spacecraft hub radius R for a tangential deployment. The derived tether inertia for each case is included in later sections. The spacecraft is modeled with the additional mass of the stowed portion of the tethers placed along the circumference of the spacecraft. Combining the time varying stowed tether contribution of the inertia to the spacecraft, the inertia of the hub is expressed in the tether fixed $\mathcal{S}$ frame, where only the third axis term will be of a contributor to the planar deployment. This third axis term expressed in the tether frame is the same for all deployment models, where m_H is the hub mass.

$$I_{s_{33}} = \frac{1}{2} m_H R^2 + R^2 (m_{T,0} - m_T) \tag{3}$$

Equations of Motion via Lagrange's Equation

The equations of motion for each case are efficiently determined using the Lagrange energy based approach. The kinetic energy of the system is

$$T = T_H + \sum_{i=1}^{N} T_{T,i} + \sum_{i=1}^{N} T_{E,i} = T_H + T_T + T_E \tag{4}$$

where subscript H refers to the spacecraft hub, T refers to the tethers, E refers to the tether end mass, and i indicates an individual tether. Assuming that all N tethers are deployed at equal rates and have identical construction, these summation terms can be reduced to a single lumped term, where the energy contribution of the tether system is equivalent to a single tether of equivalent mass. Similarly, the energy contribution of the end masses is condensed. The kinetic energy of each component is written as follows:

$$T_H = \frac{1}{2} \boldsymbol{\omega}_{\mathcal{B}/\mathcal{N}}^{\intercal} [I_s] \boldsymbol{\omega}_{\mathcal{B}/\mathcal{N}} \tag{5a}$$

$$T_T = \frac{1}{2} \boldsymbol{\omega}_{\mathcal{S}/\mathcal{N}}^{\intercal} [I_T] \boldsymbol{\omega}_{\mathcal{S}/\mathcal{N}} + \frac{1}{2} m_T \dot{\boldsymbol{R}}_{T,C} \cdot \dot{\boldsymbol{R}}_{T,C} \tag{5b}$$

$$T_E = \frac{1}{2} m_E \dot{\boldsymbol{R}}_E \cdot \dot{\boldsymbol{R}}_E \tag{5c}$$

The equations of motion are then derived using Lagrange's Equations, which state

$$\frac{\mathrm{d}}{\mathrm{d}t} \left(\frac{\partial \mathcal{L}}{\partial \dot{q}_j} \right) - \left(\frac{\partial \mathcal{L}}{\partial q_j} \right) = Q_{\mathrm{nc}_j} \tag{6}$$

If there are no potential energy sources, Lagrange's Equations are simplified to

$$\frac{\mathrm{d}}{\mathrm{d}t}\left(\frac{\partial T}{\partial \dot{q}_j}\right) - \left(\frac{\partial T}{\partial q_j}\right) = Q_{\mathrm{nc}_j} \tag{7}$$

where the non-conservative force is the torque applied on the spacecraft hub. The contribution of this torque to each general coordinate equation is determined as follows.

$$Q_{\mathrm{nc}_j} = \boldsymbol{u}_s \cdot \frac{\partial \boldsymbol{\omega}_{\mathcal{B}/\mathcal{N}}}{\partial \dot{q}_j} \tag{8}$$

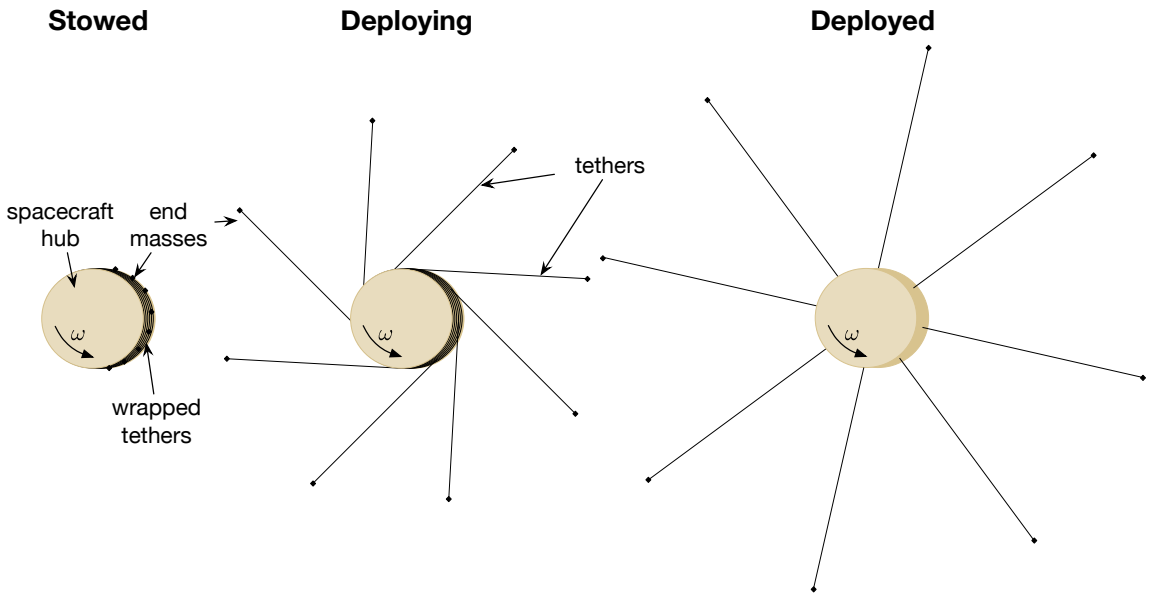

Figure 2. Diagram showing various stages of the tangential deployment scheme

Tangential Unwrap Dynamics

In this concept, the tethers are deployed tangentially using a free deployment, where the acceleration of the end mass advances the tether, much like with a yo-yo despinner. The phases of this deployment are illustrated in Figure 2. Each of the tethers are wrapped about a central hub and are unreeled from the hub simultaneously. This method takes advantage of the spin stabilized system dynamics to actuate the deployment and relies only on the spacecraft spin rate. Therefore, control of the spacecraft spin rate will couple with the deployment rate, creating a more complex dynamical system but providing a free deployment scheme. Additionally, transitioning the fully deployed tangential tethers to a radial configuration must also be modeled. Therefore, the deployment is operated in two phases, an unwrap phase that releases the tether length, and a hinging phase that transitions the tethers from the tangential to radial configurations.

The positions of the end mass and the tether center of mass are described in the $\mathcal{S} : \{\hat{\boldsymbol{s}}_1, \hat{\boldsymbol{s}}_2, \hat{\boldsymbol{s}}_3\}$ frame, where $\hat{\boldsymbol{s}}_1$ is the tether deployment direction, $\hat{\boldsymbol{s}}_2$ points to the tangent point, and $\hat{\boldsymbol{s}}_3$ is out of

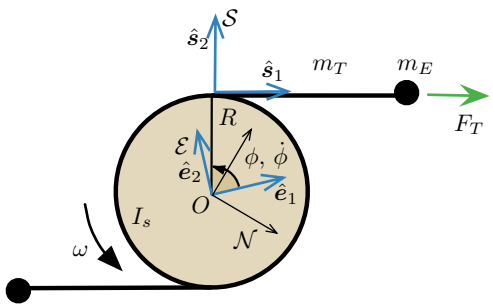

Figure 3. Tangential deployment dynamics parameters

the deployment plane.

$$\boldsymbol{R}_E = R\phi\hat{\boldsymbol{s}}_1 + R\hat{\boldsymbol{s}}_2 \tag{9}$$

$$\boldsymbol{R}_{T,C} = \frac{1}{2}R\phi\hat{\boldsymbol{s}}_1 + R\hat{\boldsymbol{s}}_2 \tag{10}$$

Here ϕ is the deployment unwrap angle, measured from the tether tangent point's original position. The velocity of the end mass and tether center of mass are next determined using the Transport Theorem,[15] where the rotation rates with respect to the inertial frame are known to be

$$\boldsymbol{\omega}_{\mathcal{B}/\mathcal{N}} = \omega\hat{\boldsymbol{s}}_3 \tag{11}$$

$$\boldsymbol{\omega}_{\mathcal{S}/\mathcal{N}} = (\omega + \dot{\phi})\hat{\boldsymbol{s}}_3 \tag{12}$$

where ω is the spacecraft spin rate and $\dot{\phi}$ is the deployment rate. The transport theorem states:[15]

$$\dot{\boldsymbol{R}}_E = \frac{^{\mathcal{N}}\mathrm{d}}{\mathrm{d}t}(\boldsymbol{R}_E) = \frac{^{\mathcal{B}}\mathrm{d}}{\mathrm{d}t}(\boldsymbol{R}_E) + \boldsymbol{\omega}_{\mathcal{S}/\mathcal{N}} \times \boldsymbol{R}_E \tag{13}$$

Then the velocity vectors are determined as

$$\dot{\boldsymbol{R}}_E = -R\omega\hat{\boldsymbol{s}}_1 + R\phi(\omega + \dot{\phi})\hat{\boldsymbol{s}}_2 \tag{14}$$

$$\dot{\boldsymbol{R}}_{T,C} = -\frac{1}{2}R(2\omega + \dot{\phi})\hat{\boldsymbol{s}}_1 + \frac{1}{2}R\phi(\omega + \dot{\phi})\hat{\boldsymbol{s}}_2 \tag{15}$$

Treating the inertia of the tether as a slender rod, and applying the parallel axis theorem, the inertia of the tethers with respect to an origin located at the spacecraft center of mass is shown in Eq. (16), expressed in the tether fixed $\mathcal{S}$ frame.

$$[I_T] = [I_{T,C}] + m_T[\tilde{\boldsymbol{R}}_{T,C}][\tilde{\boldsymbol{R}}_{T,C}]^\intercal \tag{16}$$

$$[I_T] = \begin{bmatrix} R^3\rho\phi & -\frac{1}{2}R^3\rho\phi^2 & 0 \\ -\frac{1}{2}R^3\rho\phi^2 & \frac{1}{3}R^3\rho\phi^3 & 0 \\ 0 & 0 & \frac{1}{12}R^3\rho\phi^3 + R\rho\phi(R^2 + \frac{1}{4}R^2\phi^2) \end{bmatrix} \tag{17}$$

The generalized coordinates are chosen as the angular position description of the spacecraft hub and the tether deployment, where $\theta = \omega t$.

$$\begin{bmatrix} q_1 & q_2 \end{bmatrix} = \begin{bmatrix} \theta & \phi \end{bmatrix} \tag{18}$$

Using Eqs. (9) - (17) in the Lagrange's Equation algorithm of Eqs. (4) - (8), the equations of motion are determined.

$$\frac{1}{24}R^2(-3(4R\rho+8m_E\phi+7R\rho\phi^2)\omega^2+3(5R\rho+8m_E\phi+7R\rho\phi^2)\dot{\phi})+$$
$$\frac{1}{12}R^2\phi(18R\rho+12m_E\phi+7R\rho\phi^2)\dot{\omega}+$$
$$\frac{1}{12}R^2\phi(15R\rho+12m_E\phi+7R\rho\phi^2)\ddot{\phi}=0 \quad (19)$$

$$\frac{1}{12}R^2(3(4R\rho+8m_E\phi+7R\rho\phi^2)\omega\dot{\phi}+3(6R\rho+8m_E\phi+7R\rho\phi^2)\dot{\phi}^2)+$$
$$\frac{1}{12}R^2(6(2m_E+m_H+2m_{T,0})+12R\rho\phi+12m_E\phi^2+7R\rho\phi^3)\dot{\omega}+$$
$$\frac{1}{12}R^2\phi(18R\rho+12m_E\phi+7R\rho\phi^2)\ddot{\phi}=u_s \quad (20)$$

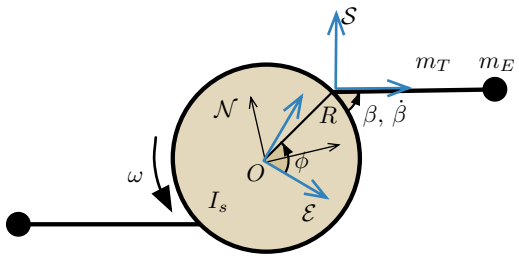

Figure 4. Hinging from tangential to radial dynamics parameters

Tangential Hinging Dynamics

Considering the hinging phase of the tangential deployment, and using similar methods as those described above, the hinge phase equations of motion are also determined. The parameters of interest are defined in Figure 4. The tether has freedom to rotate about the connection point by angle β, where the desired dynamics will come to rest at $\beta = 90\,\text{deg}$. The deployment angle ϕ is now fixed constant. The positions of the end mass and the tether center of mass are now described in the $\mathcal{S}$ frame.

$$\boldsymbol{R}_{E,H} = R\phi\hat{\boldsymbol{s}}_1 + R\hat{\boldsymbol{e}}_2 \quad (21)$$
$$\boldsymbol{R}_{T,H} = \frac{1}{2}R\phi\hat{\boldsymbol{s}}_1 + R\hat{\boldsymbol{e}}_2 \quad (22)$$

Using Eq. (13), where the relative rate is Eq. (23), the velocity vectors are determined.

$$\boldsymbol{\omega}_{\mathcal{S}/\mathcal{N}} = (\omega+\dot{\beta})\hat{\boldsymbol{s}}_3 \quad (23)$$
$$\dot{\boldsymbol{R}}_{E,H} = R\phi\hat{\boldsymbol{s}}_1 \quad (24)$$
$$\dot{\boldsymbol{R}}_{T,H} = -R\cos\beta\omega\hat{\boldsymbol{s}}_1 + \frac{1}{2}R((\phi+2\sin\beta)\omega+\phi\dot{\beta})\hat{\boldsymbol{s}}_2 \quad (25)$$

The tether inertia for this phase is determined using Eq. (16), where the hinging position description is used. Only the third axis inertia is included in the planar dynamics.

$$I_{T,H_{33}} = \frac{1}{3}R^3\rho\phi(3+\phi^2+3\phi\sin\beta) \tag{26}$$

Selecting the general coordinates to be the spacecraft position angle and the hinging angle, $q_1 = \theta$ and $q_2 = \beta$, and using Eqs. (21) - (26) in the Lagrange's Equation algorithm of Eqs. (4) - (8), the equations of motion are determined.

$$\begin{aligned}\frac{1}{2}R^2\phi\cos\beta(-2(m_E+R\rho\phi)\omega^2+R\rho\phi\dot{\beta}^2)+\\ \frac{1}{12}R^2\phi(12m_E\phi+R\rho(12+7\phi^2)+6(2m_E+3R\rho\phi)\sin\beta)\dot{\omega}+\\ \frac{1}{12}R^2\phi(12m_E\phi+R\rho(12+7\phi^2)+12R\rho\phi\sin\beta)\ddot{\beta}=0\end{aligned} \tag{27}$$

$$\begin{aligned}\frac{1}{12}R^2(24\phi(m_E+R\rho\phi)\cos\beta\omega\dot{\beta}+6\phi(2m_E+3R\rho\phi)\cos\beta\dot{\beta}^2)+\\ \frac{1}{12}R^2(6m_H+12m_{T,0}+12m_E(1+\phi^2)+R\rho\phi(12+7\phi^2)+24\rho(m_E+R\rho\phi)\sin\beta)\dot{\omega}+\\ \frac{1}{12}R^2\phi(12m_E\phi+R\rho(12+7\phi^2)+6(2m_E+3R\rho\phi)\sin\beta)\ddot{\beta}=u_s\end{aligned} \tag{28}$$

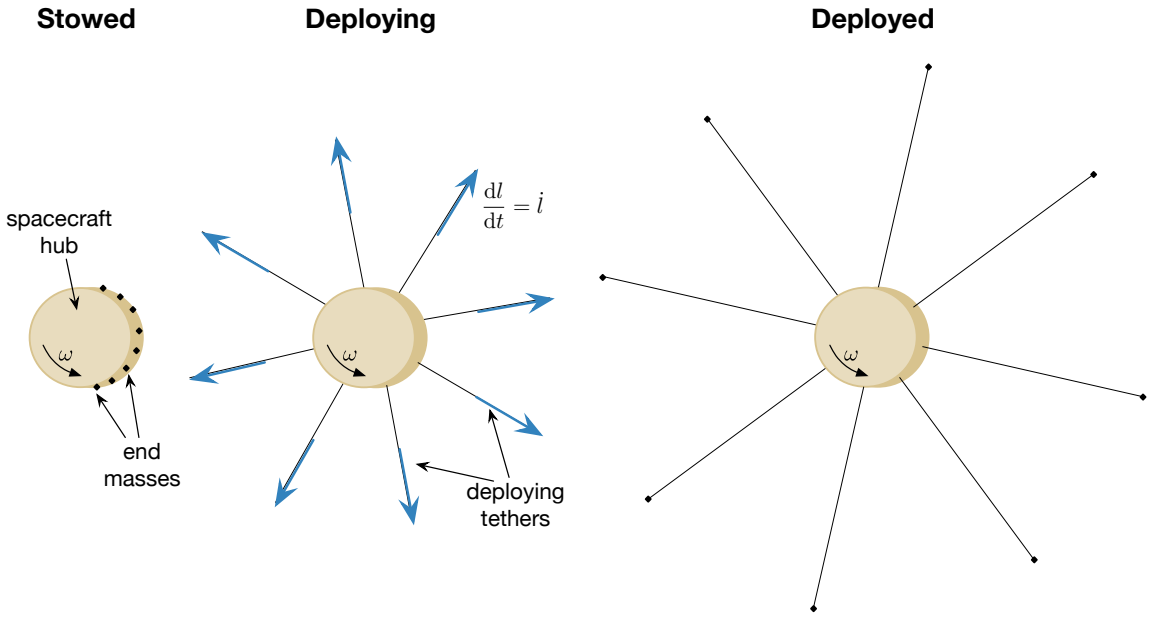

Figure 5. Various stages of the radial deployment scheme

Radial Deployment Dynamics

Another method for deployment would be to use radially deploying tethers, as seen in Figure 5. Such a design requires tether reeling modules to stow and control each of the 20-100 tethers individually, and therefore requires 20-100 drive mechanisms. This introduces a large power consumption during the deployment as well as synchronization challenges. Additionally, the system still experiences significant momentum exchange and rate changes that couples with the unreeling process. However, this method enables independent control of the tethers and decouples deployment failure risks of the tethers from each other. Furthermore, substantial engineering development has been done on a reeling mechanism.[12] Energy methods are used to determine the equations of motion for the radial deployment case.

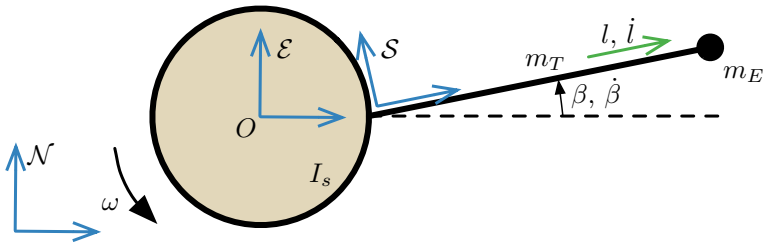

Figure 6. Radial deployment dynamics parameters

The positions of the end mass and the tether center of mass are described in the $\mathcal{S}$ frame, illustrated in Figure 6, as

$$\boldsymbol{R}_{E,H} = l\hat{\boldsymbol{s}}_1 + R\hat{\boldsymbol{e}}_1 \tag{29}$$

$$\boldsymbol{R}_{T,H} = \frac{1}{2}l\hat{\boldsymbol{s}}_1 + R\hat{\boldsymbol{e}}_1 \tag{30}$$

Here β is the angle of deviation of the tether from radial, and $\dot{\beta}$ is the rotation rate of the tether, the tether rotation with respect to inertial is

$$\boldsymbol{\omega}_{\mathcal{S}/\mathcal{N}} = (\omega + \dot{\beta})\hat{\boldsymbol{s}}_3 \tag{31}$$

Using (13), where the rotation rate is (31), the velocity vectors are determined as

$$\dot{\boldsymbol{R}}_{E,H} = (\dot{l} + R\sin\beta\omega)\hat{\boldsymbol{s}}_1 + (l(\dot{\beta} + \omega) + R\cos\beta\omega)\hat{\boldsymbol{s}}_2 \tag{32}$$

$$\dot{\boldsymbol{R}}_{T,H} = \left(\frac{1}{2}\dot{l} + R\sin\beta\omega\right)\hat{\boldsymbol{s}}_1 + \left(\frac{1}{2}l(\dot{\beta} + \omega) + R\cos\beta\omega\right)\hat{\boldsymbol{s}}_2 \tag{33}$$

The radial tether inertia of the third axis is determined using (16):

$$I_{T,H_{33}} = \frac{1}{12}\rho l^3 + \rho l((R\cos\beta + \frac{1}{2}l)^2 + R^2\sin\beta^2) \tag{34}$$

Selecting the general coordinates to be the spacecraft position angle and tether hinging angle, $q_1 = \theta$ and $q_2 = \beta$, and using Eqs. (29) - (34) in the Lagrange's Equation algorithm of Eqs. (4) - (8), the

equations of motion are determined.

$$\frac{1}{12}(6R\rho\sin\beta\dot{l}^2 - 12Rl\sin\beta m_E\dot{\beta}(\dot{\beta}+2\omega) - 6R\rho l^2\sin\beta\dot{\beta}(3\dot{\beta}+4\omega))+$$
$$\frac{1}{12}(3\dot{l}((4R^2\rho+7\rho l^2+8lm_E)(\dot{\beta}+\omega)+2R\cos\beta(4m_E(\dot{\beta}+\omega)+\rho l(7\dot{\beta}+8\omega))))+$$
$$\frac{1}{12}(12R^2\rho l+24R\rho\cos\beta l^2+7\rho l^3+24R\cos\beta lm_E+12l^2m_E+6R^2(2m_E+m_H+2m_{T,0}))\dot{\omega}+$$
$$\frac{1}{12}(12R^2\rho l+18R\rho\cos\beta l^2+7\rho l^3+12R\cos\beta lm_E+12l^2m_E)\ddot{\beta}=u_s \quad (35)$$

$$\frac{1}{12}(6Rl\sin\beta(-\rho l\dot{\beta}^2+2(\rho l+m_E)\omega^2))+$$
$$\frac{1}{12}(3\dot{l}((4R^2\rho+7\rho l^2+8lm_E)(\dot{\beta}+\omega)+2R\rho\cos\beta l(4\dot{\beta}+5\omega)))+$$
$$\frac{1}{12}(6R\cos\beta l(3\rho l+2m_E)+l(12R^2\rho+7\rho l^2+12lm_E))\dot{\omega}+$$
$$\frac{1}{12}(12R\rho\cos\beta l^2+l(12R^2\rho+7\rho l^2+12lm_E))\ddot{\beta}=0 \quad (36)$$

CONTROL DEVELOPMENT

The goal of the deployment control scheme is to determine if the desired deployment behavior can be achieved using only one torque actuation source located on the spacecraft hub and closed loop feedback control. Placing the deployment control actuation on the tethers directly would introduce many complex challenges. Up to 100 actuators would require rapid simultaneous sensing and commanding and fuel consumption for the deployment would reduce the fuel available for subsequent E-sail operations. The ability to input the energy and momentum through hub mounted thrusters provides a practical solution to the deployment requirements.

Controllability Analysis

To provide preliminary evaluation of the controllability of the radial deployment through an applied torque on the spacecraft hub, linearized time invariant models of the tangential and radial deployment models are developed. Each system of equations is first reduced such that the length of the tether is fixed. This simplification assumes the length rate is negligible. The ideal deployment configuration, where the tether does not deviate from the desired orientation and the spacecraft is rotating at a prescribed rate, provides the reference point for the linearization. The nonlinear systems of equations are approximated using the Taylor series expansion in Eq. (37), where higher order terms are neglected.

$$\dot{\boldsymbol{x}} \simeq \frac{\partial f(\boldsymbol{x}_r,\boldsymbol{u}_r)}{\partial \boldsymbol{x}}\boldsymbol{x} + \frac{\partial f(\boldsymbol{x}_r,\boldsymbol{u}_r)}{\partial \boldsymbol{u}}\boldsymbol{u} \simeq [A]\boldsymbol{x} + [B]u_s \quad (37)$$

where $\boldsymbol{x}$ is the radial deployment state vector

$$\boldsymbol{x} = \begin{bmatrix}\omega & \beta & \dot{\beta}\end{bmatrix} \quad (38)$$

and Eqs (35)-(36) are written in the standard form

$$\dot{\boldsymbol{x}} = f(\boldsymbol{x},\boldsymbol{u}) \quad (39)$$

System controllability is evaluated by verifying the controllability matrix is of full rank. Where the number of states in each model is $n = 3$, the controllability matrix is formed as

$$\begin{bmatrix} C \end{bmatrix} = \begin{bmatrix} B & AB & A^2B \end{bmatrix} \tag{40}$$

where the 3×3 $[A]$ and 3×1 $[B]$ matrices are the Jacobians defined in Eq. (37) and are determined analytically. The analytical solutions are omitted here for brevity. It is determined that a single control input on the spacecraft hub provides a controllable system for cases operating near their reference point with a very slow deployment rate.

Control Algorithm

Initial control schemes shown here use simple proportional-integral-derivative (PID) control algorithms to affect the system behavior. Time invariant gains are used for the following simulations. For the tangential unwrap and radial cases, the controller will feedback on the spacecraft rate to follow the desired rate trajectory.

$$u_{s_i} = K_P(\omega_i - \omega_r) + K_D \frac{\omega_i - \omega_{i-1}}{dt} + K_I \int_0^t (\omega_i - \omega_r) dt \tag{41}$$

where K_P, K_D, and K_I are control gains. Here the tether deployment dynamics are treated as an unmodeled torque, requiring high gains to compensate for the unpredicted behavior. Achieving the desired spin rate becomes more challenging through the deployment as the inertia of the tethers increases, therefore increasing the contribution of the unmodeled dynamics. Using time varying gains could help address this issue and is left for future work. For the tangential hinging phase, a PID controller with tether position feedback is used.

Spacecraft Rate Considerations

The spacecraft spin rate trajectory about the deployment spin axis is a critical condition in the deployment simulations. There are two factors to consider to determine the ideal rate - the internal tether tension force and spin rate trajectory curves.

Tether Tension An expression for the internal tether tension force is derived from the force balance equations on the tether end mass. A maximum acceptable tether tension force is determined from the strength of the conducting material. In tensile strength testing of a prototype Hoytether, the maximum tensile strength was found to be 0.4-0.5 N.[12] The baseline Hoytether has a maximum usable tension of 0.05 N, when considering the bonds between the main and redundant tether loops.[16] The expression for tether tension in the tangential model is defined as

$$F_{T_T} = m_{E,i} R(\phi(\omega + \dot{\phi})^2 + \dot{\omega}) \tag{42}$$

and the tension force is similarly determined for the radial deployment as

$$F_{T_R} = m_{E,i}(R\cos\beta\omega^2 + l(\dot{\beta} + \omega)^2 - \ddot{l} - R\sin\beta\dot{\omega}) \tag{43}$$

Tangential Deployment Spin Rate Trajectories The reference trajectories of the spacecraft spin rate will strongly affect the deployment behavior, where the torque, tether tension, and deployment rates vary under different trajectories. While it is simplest to set trajectories that maintain a constant desired rate, there are advantages to considering nonlinear trajectories for the spacecraft rate. For

an uncontrolled deployment, the spacecraft rate is exponentially driven to approach the negative of the initial rate. This drop in spacecraft rate quickly transfers momentum to the deploying tethers, however a negative spacecraft rate is highly undesirable, where tension is no longer maintained. The concept of permitting the spacecraft rate to spin down slightly to transfer momentum to the tethers can be implemented by setting a reference trajectory that follows an exponential decay towards a desired final rate. Such a trajectory can be written as follows, where c is a constant that scales the rate of decay.

$$\omega_{ref} = (\omega_0 - \omega_f)e^{-t/c} + \omega_f \tag{44}$$

SIMULATION RESULTS

The following baseline E-sail and spacecraft model is used to demonstrate the behavior of both the tangential and radial simulations. Differences in behavior for the two models will become apparent through studying multiple case runs, however this shows the general trends of deployment. The E-sail described in Table 1 represents an E-sail with the smallest inertia for the smallest characteristic acceleration under consideration. Subsequently, the deployment behaviors shown are representative of the lower bound for torque requirements and deployment time. The end mass is minimal and represents the case where no auxiliary tether or remote thrusters are used. Control of individual tethers in this case would be achieved using mass efficient photonic blades[17] or other mass efficient methods if needed.

Table 1. Spacecraft and E-sail parameters implemented in both example simulations are chosen to minimize E-sail inertia.

$a_\oplus$ mm/s^2	N	L m	m_{E_i} kg	m_T kg	m_H kg
0.1	100	862.3	0.05	0.996	500

Tangential Model

Sample results are provided in Figure 7 for a controlled simulation of the tangential unwrap deployment with a hinging transfer to the desired configuration demonstrated in Figure 8. The parameters used in this case are recorded in Table 1. The initial spin rate is chosen such that the tether tension does not exceed 0.05 N at the end of deployment. The spacecraft rate trajectory is held constant throughout. It's shown that the deployment is completed in just 1.3 days for this small E-sail model. The inertia and angular momentum grows nonlinearly through the deployment, as expected from the inertia derivation discussed earlier. For this small E-sail model, the tether inertia is approximate 7% of the end mass inertia. However, for much larger E-sails, the tether inertia is comparable to the end mass inertia contribution. The torque effort needed to maintain the constant desired hub rate increases linearly to 1.17 Nm, which can be achieved by applying a couple moment through time varying electric thrusters about the hub radius. The tether tension grows linearly to 0.01 N, well below the approximate operable max of 0.05 N. As seen in Figure 8, the time to correct the tether orientation is less than 20 minutes. The controller can enforce a slower transition, but a torque effort must be applied. The torque required for this transition peaks at 1.2 Nm, around the same range as the deployment phase and therefore within the required torque capabilities.

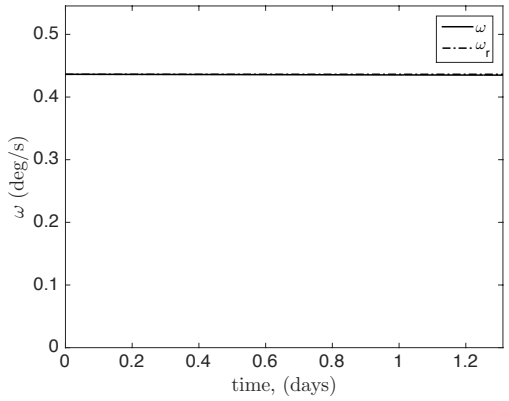

(a) body rate

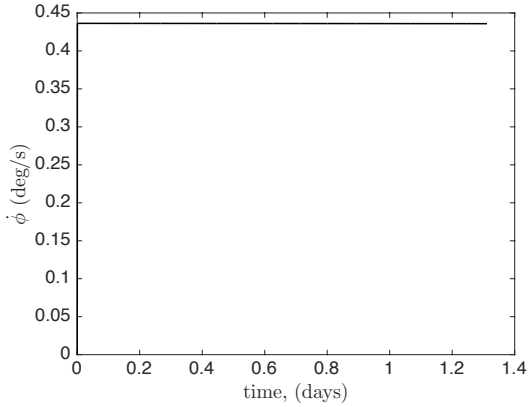

(b) unwrap rate

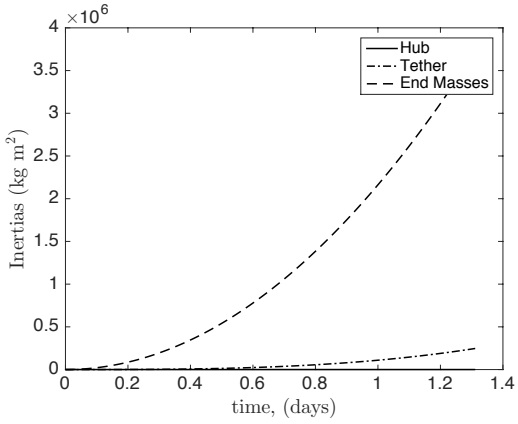

(c) inertia of each component

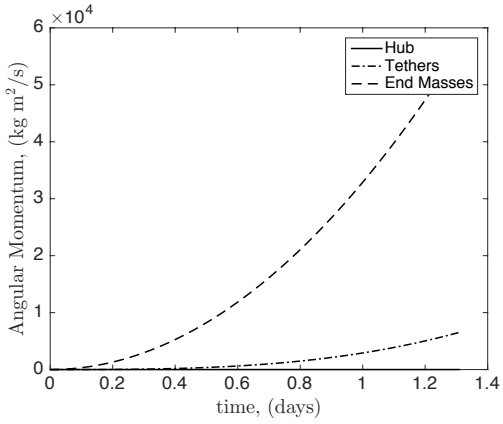

(d) angular momentum of each component

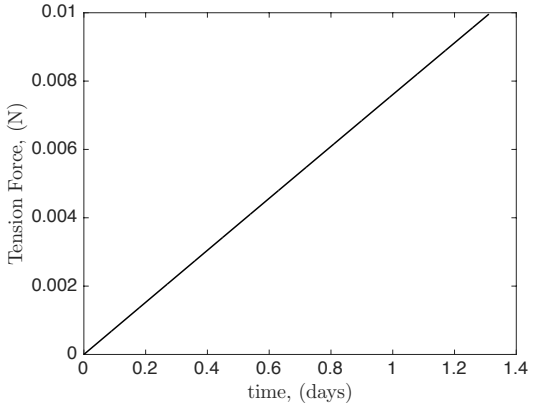

(e) tension force in each tether

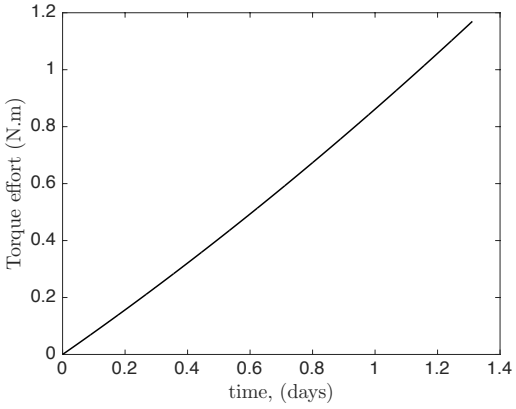

(f) torque required

Figure 7. Unwrap phase deployment states of the tangentially deployed E-sail

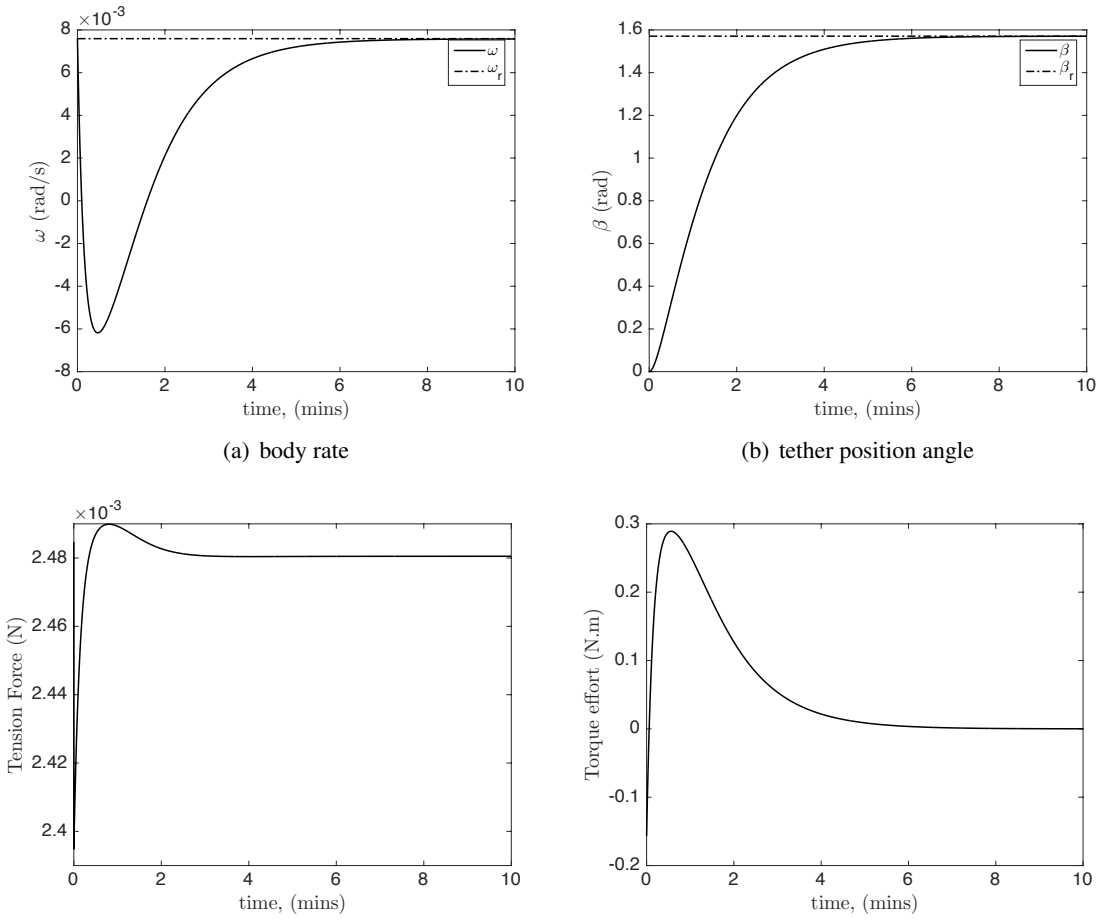

(a) body rate

(b) tether position angle

(c) tension force in each tether

(d) torque required

Figure 8. Hinging phase deployment states of the tangentially deployed E-sail

Radial Model

Sample results from the radial model are displayed in Figure 9. The tether deployment rate, $\dot{l}$, is set to a constant rate such that the time of the deployment is equal to the previous tangential case. Maintaining a radial configuration, where the tether relative position angle, β, is near zero with respect to the spacecraft hub, requires a high spacecraft spin rate that results in an unacceptably large tether tension force of 1.7 N for this case. Additionally, the torque required to maintain such a configuration is over 15 N.m, ten times greater. Therefore, it is not possible to deploy at a purely radial configuration in the same time frame as for the tangential case using constant spin rate control. The relative angle, β, must be allowed to drift such that the tether tension is not above 0.05 N. Practical implementation of such a deployment would need to identify acceptable bounds for β. Alternatively, the deployment could be conducted with much slower deployment rate to maintain a radial configuration. Maintaining the same spin rate as the tangential case, and slowing down the deployment until β is less than 5 degrees, the deployment needs up to 50 times longer, or 66 days, to complete. This long deployment duration raises consideration for why a purely radial deployment orientation would be desired, and motivates allowing some hinging during the deployment.

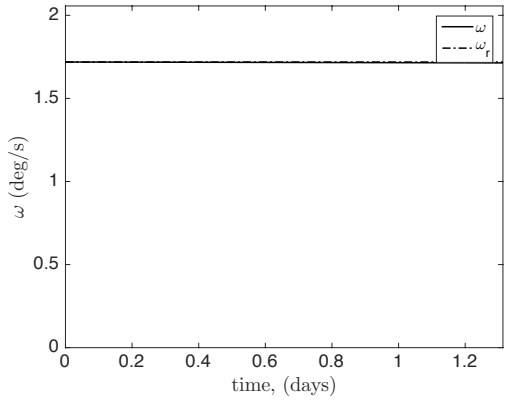

(a) body rate

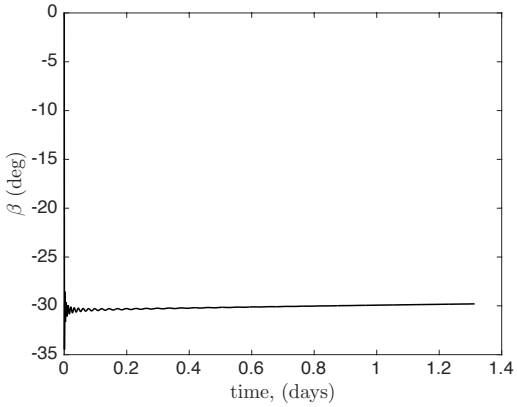

(b) tether position angle

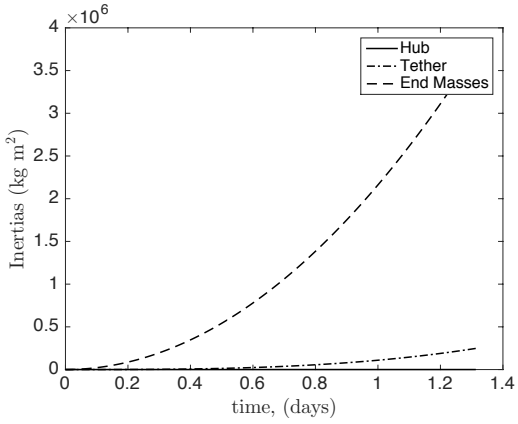

(c) component inertia

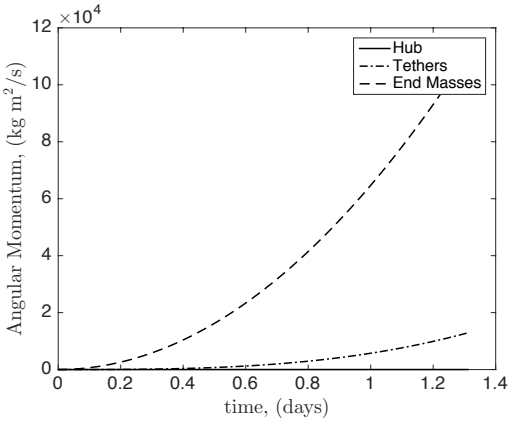

(d) component momentum

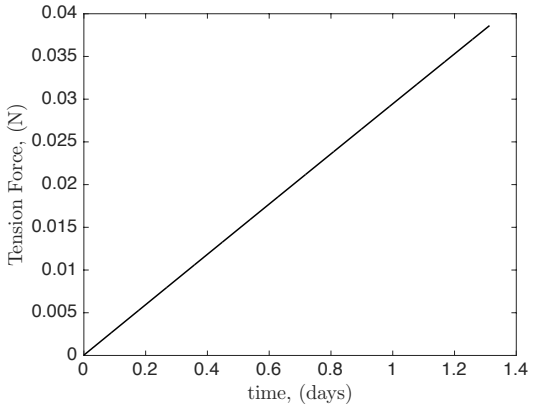

(e) tension force in each tether

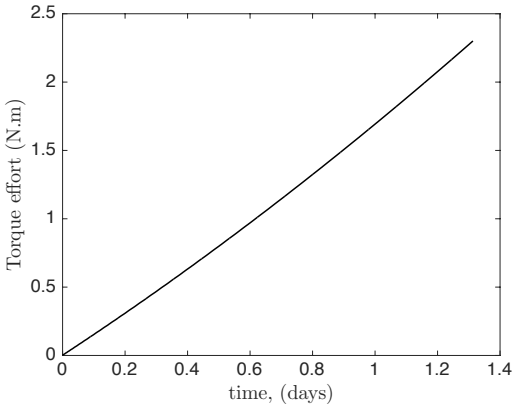

(f) torque required

Figure 9. Deployment states of the radially deployed E-sail

Tangential Deployment Parameter Study

The tangential model is now adapted for several cases of characteristic accelerations and E-sail sizes to determine torque and deployment time, shown in Table 2. The radial model is not yet considered for a parameter study because of the large variations in deployment behavior based on initial conditions and β requirements. The hub spin rate is set such that the final tension in the tethers, F_{T_f}, is equal to the maximum operable tension. This suggests a minimal deployment time for a constant spin rate trajectory deployment, where a slower deployment would result in lower tension force. The deployment time, t_d, is shown to increase dramatically for large E-sails with longer tethers, taking over two months for some cases. While using fewer short tethers for the same characteristic acceleration would mean fewer individual tethers to actuate and fabricate, the trade is needing more time to deploy. All cases in Table 2 have a total spacecraft mass of $m = 500$ kg and end masses of $m_{E,i} = 50$ g. Note that larger end masses will produce higher tension force on the tethers, requiring slower deployments.

Table 2. Tangential deployment behavior for various E-sails

$a_\oplus$ mm/s^2	ω deg/s	N	L km	m_T kg	$u_{s,max}$ N.m	F_{T_f} N	t_d days
0.1	0.98	100	0.86	1.00	5.89	0.050	0.58
0.1	0.69	50	1.72	1.00	3.34	0.050	1.66
0.1	0.44	20	4.31	1.00	1.86	0.050	6.56
0.1	0.31	10	8.62	1.00	1.37	0.050	18.47
0.5	0.43	100	4.31	4.98	9.08	0.049	6.57
0.5	0.31	50	8.62	4.98	6.89	0.050	18.25
0.5	0.19	20	21.16	4.98	5.46	0.050	71.41
1.0	0.30	100	8.62	9.96	13.74	0.050	18.25
1.0	0.21	50	17.25	9.96	11.30	0.050	50.66

SPACECRAFT RATE TRAJECTORY IN TANGENTIAL DEPLOYMENT

The nonlinear reference trajectory shown in Eq. (44) is applied to a tangential deployment that shares all other parameters as the case shown in Figure 7. The decay rate constant c adjusted to optimize the results. The spacecraft is spun up to a rate 6 times greater than the desired final rate. Figure 10 shows that the deployment is achieved using the same range of torques in 0.889 days, or 32% less time than a constant trajectory case. This can be advantageous for larger E-sail deployments, where the deployment time can take up to a few months.

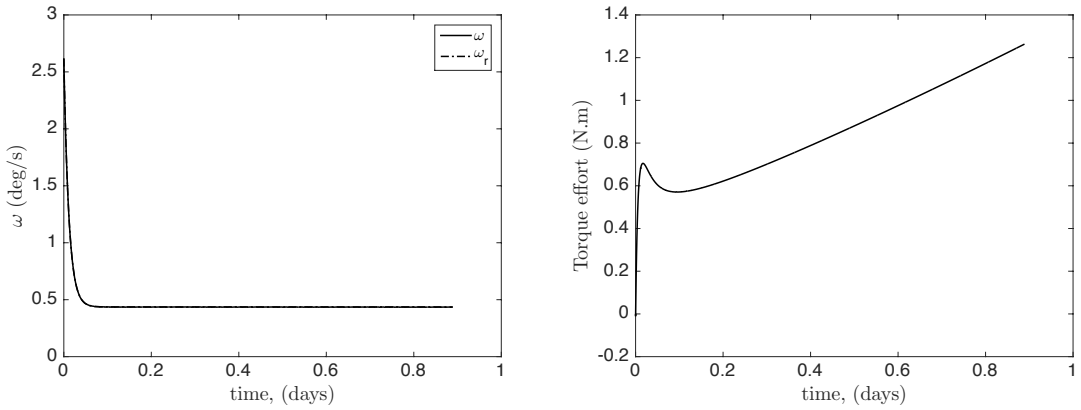

(a) spacecraft spin rate and rate trajectory (b) torque required

Figure 10. Tangential deployment using a nonlinear reference trajectory

CONCLUSIONS AND FUTURE WORK

The two E-sail deployment schemes investigated in this paper provide feasible means to actuate the deployment of an E-sail structure using hub mounted torque only. The tangential deployment scheme provides a simpler deployment for lower torque, however it removes the ability to control the individual tether spooling. Deployment in a truly radial configuration, where $\beta = 0$, is shown to require much greater spin rates or much longer deployment duration than allowing tethers to drift. The advantage of an ideal radial deployment is that a hinge phase would not be needed, however in practical application it is shown that allowing hinging will greatly reduce the deployment time or hub spin rate requirements. The radial deployment configuration was developed based on the individual tether spooling concept. Modifying the individual spools to orient the deployment to a tangential configuration would be worth considering in future simulations, and may provide the optimal deployment.

The deployment torque can be applied to the hub using a variety of methods, depending on the order of magnitude and duration of torque needed for the deployment. Electric thrusters are ideal candidates for their range of thrust magnitudes and time varying capabilities for smaller inertia E-sails. Reaction wheels could also be used if fine control is needed, however the momentum stored in the wheels would need to be actively removed through thrusters. Chemical thrusters may also be used to achieve large torques for large E-sails, however the time variations could only be achieved using pulse width modulation thrust. The effects of such an approach on the deployment dynamics must be investigated to ensure stability. Incorporating realistic thruster models to the deployment simulation is left to future work.

The spacecraft rate trajectory, deployment rate, characteristic acceleration, and tether tip mass are large contributors to the deployment dynamics and must be chosen judiciously. Defining realistic boundaries for these parameters based on technology capabilities and mission requirements will inform future simulations. Additionally, it is determined that E-sails designed to have a greater number of shorter tethers have smaller inertia and therefore require less energy and momentum to deploy. However, these tethers would be in closer proximity to each other and may present collision risks. State error estimation of the tether positions must be done to determine the closest

allowable proximity of two adjacent tethers. Future work will model each tether individually with a unique state and determine the factors influencing variation in position to do this. Permitting tether hinging raises concern that the flexible tethers may exhibit in-plane bending despite internal tension. Model fidelity will therefore be further increased by using a lumped-mass method to incorporate the flexibility of the tethers. While many questions on the finer behavior of the E-sail deployment remain, the baseline momentum and torque requirements of the hub actuated deployment are now defined.

REFERENCES

[1] P. Janhunen, "Electric Sail for Spacecraft Propulsion," *Journal of Propulsion and Power*, Vol. 20, No. 4, 2004.

[2] P. Janhunen, "The electric sail - a new propulsion method which may enable fast missions to the outer solar system," *Journal of the British Interplanetary Society*, Vol. 61, No. 8, 2008, pp. 326–329.

[3] P. Janhunen and A. Sandroos, "Simulation study of solar wind push on a charged wire: basis of solar wind electric sail propulsion," *Annales Geophysicae*, Vol. 25, 2007, pp. 755–767.

[4] R. M. Y. Les Johnson and E. E. M. IV, "Status of Solar Sail Propulsion: Moving Toward an Interstellar Probe," *AIP Conference Proceedings*, Vol. 886, 2007, pp. 207–214.

[5] A. Szames.

[6] S. M. Pekka Janhunen, J. Lebreton, "Fast E-sail Uranus entry probe mission," *Planetary and Space Science*, Vol. 104, 2014, pp. 141–146.

[7] B. Wiegmann, "Heliopause Electrostatic Rapid Transit System (HERTS)," June 2014.

[8] A. A. Quarta and G. Mengali, "Electric Sail missions to potentially hazardous asteroids," *Acta Astronautica*, Vol. 66, 2010, pp. 1506–1619.

[9] G. Mengali and A. A. Quarta, "Electric Sail Performance Analysis," *Journal of Spacecraft and Rockets*, Vol. 45, No. 1, 2008, pp. 122–129.

[10] R. Hoyt and R. L. Forward, "Alternate interconnection Hoytether failure resistant multiline tether," 2001.

[11] J. U. S. K. G. M. P. J. Timo Rauhala, Henri Seppanen and E. Hggstrom, "Automatic 4-wire Heytether production for the Electric Solar Wind Sail," *International Microelectronics Assembly and Packing Society Topical Workshop and Tabletop Exhibition on Wire Bonding*, 2013.

[12] K. T. Z. P. J. R. Rosta, O, "Wrecker: an unreeling mechanism for a thin electrically conductive space tether," *CEAS Space Journal*, Vol. 7, 2015, pp. 53–68.

[13] A. S. e. al., "ESTCube-1 in-orbit experience and lessons learned," *Aerospace and Electronic Systems Magazine, IEEE*, Vol. 30, 2015, pp. 12–22.

[14] G. M. P. Janhunen, A. Quarta, "Electric solar wind sail mass budget model," *Geoscientific Instrumentation, Methods and Data Systems*, Vol. 2, 2013, pp. 85–95.

[15] H. Schaub and J. L. Junkins, *Analytical Mechanics of Space Systems*. 1801 Alexander Bell Drive, Reston, Virginia, 20191-4344: American Institute of Aeronautics and Astronautics, Inc., 3rd ed., 2014.

[16] P. T. Pekka Janhunen, "Safety criteria for flying E-sail through solar eclipse," *Acta Astronautica*.

[17] P. Janhunen, "Photonic spin control for solar wind electric sail," *Acta Astronautica*.